Supporting Information:

Carbon-templated Conductive Oxide Supports for Oxygen Evolution Catalysis

Alexander G. Hufnagel,[†] Sebastian Häringer,[†] Michael Beetz,[†] Bernhard Böller,[†] Dina Fattakhova-Rohlfing,[‡] and Thomas Bein*[,†]

[†]*Department of Chemistry and Center for NanoScience (CeNS), University of Munich (LMU), Butenandtstraße 5-13 (E), 81377 Munich, Germany.*

[‡]*Institut für Energie- und Klimaforschung, Forschungszentrum Jülich GmbH, Wilhelm-Johnen-Straße, 52425 Juelich, Germany.*

E-mail: bein@lmu.de

Carbon Soot Template

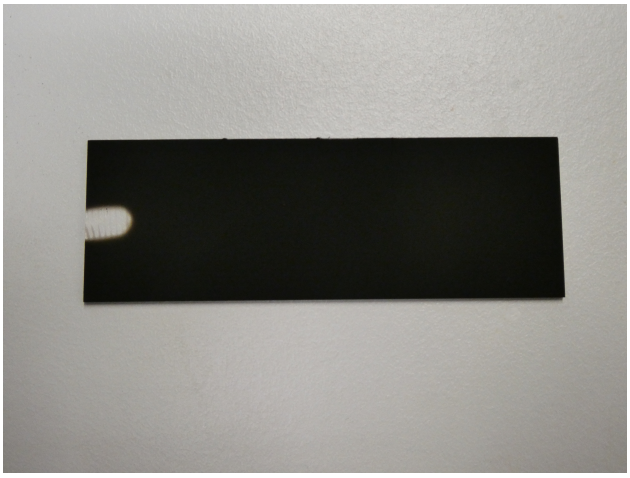

Figure S1: Photograph of as-deposited carbon soot on soda-lime glass (SLG).

Carbon NTO Scaffolds

Table S1: Compositions of NTO prepared for this study. In the cycle sequence column, Ti represents one TiO_2 ALD cycle and Nb one NbO_x ALD cycle.

Theor. composition	ALD cycle sequence	composition (EDX)
Ti:0.97; Nb:0.03	(20 x Ti + 1 x Nb) x n	Ti:0.97; Nb:0.03
Ti:0.91; Nb:0.09	(14 x Ti + 1 x Nb) x n	Ti:0.90; Nb:0.10
Ti:0.82; Nb:0.18	(6 x Ti + 1 x Nb) x n	Ti:0.80; Nb:0.20
Ti:0.75; Nb:0.25	(4 x Ti + 1 x Nb) x n	Ti:0.71; Nb:0.29

Table S2: Crystallite sizes of carbon-templated NTO films calculated using the Scherrer equation.

composition (EDX)	cr. size (as-dep.) nm	cr. size (600°C) nm	cr. size (700°C) nm
$Ti_{0.97}Nb_{0.03}O_2$	46	50	56 (rutile)
$Ti_{0.80}Nb_{0.20}O_2$	amorphous	38	29

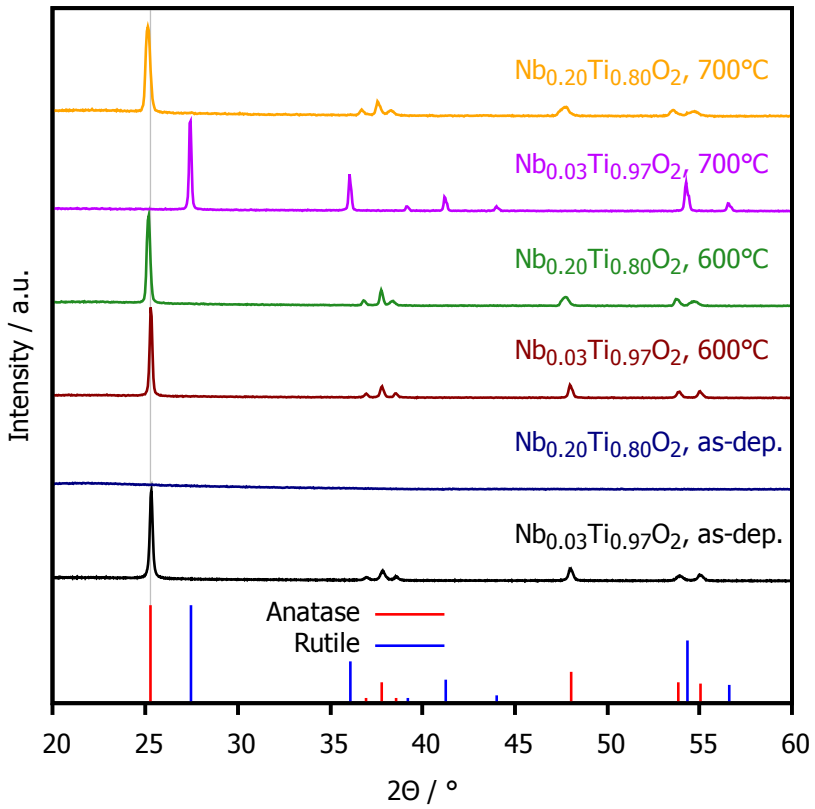

Figure S2: X-ray diffractograms of NTO-coated carbon soot samples on fused silica. The data have been normalized and offset for visual clarity.

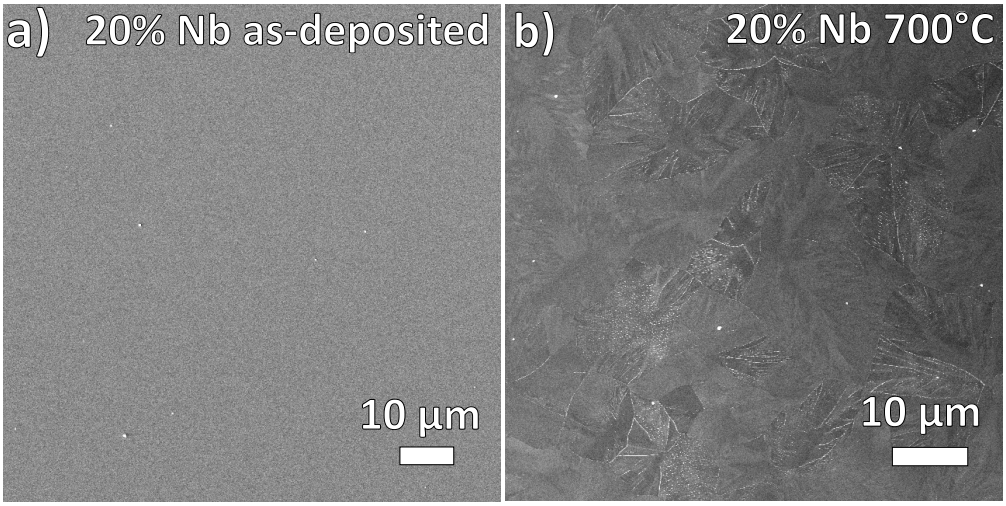

Figure S3: Top-view SEM images of a compact as-deposited NTO layer (∼80 nm, 20 % Nb) on fused silica (a). The same layer after annealing at 700°C (b).

Nitrogen sorption

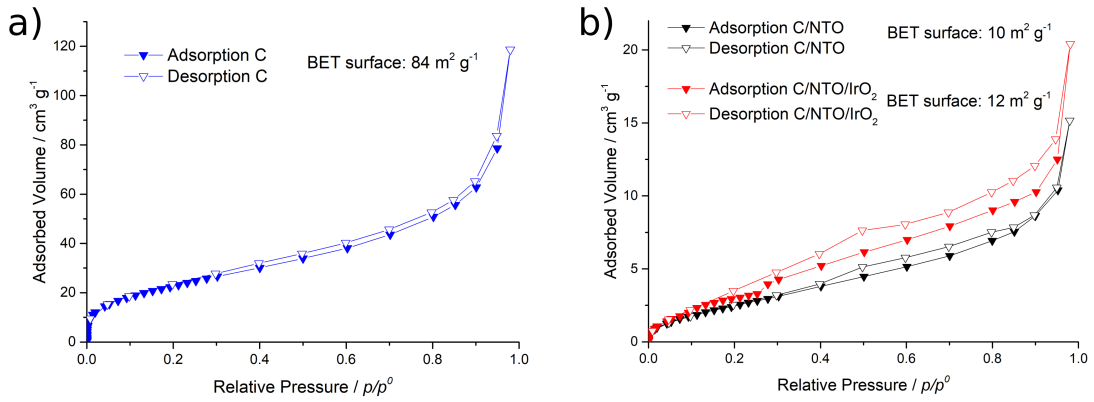

Figure S4: Nitrogen sorption isotherms of carbon soot (a), C/NTO and C/NTO/IrO_2 (b) powder samples measured at 77 K.

Figure S4 shows the nitrogen sorption isotherms recorded for pure carbon soot, NTO on carbon soot and iridium oxide on the C/NTO scaffold. The decrease of surface area per weight can be attributed to the enhanced mass of niobium-doped titanium oxide in comparison to pure carbon soot. The type II isotherm indicates a nonporous material with some textural porosity for the three different materials. Sorption data were collected on a Quantachrome Autosorb 1 at 77 K in a pressure range from $p/p_0 = 0.001$ to 0.98. The sample was heated prior to the measurement for 24 h at 120 °C under vaccum. The BET model was applied between 0.05 and 0.2 p/p_0.

Further Characterization of ALD IrO_2

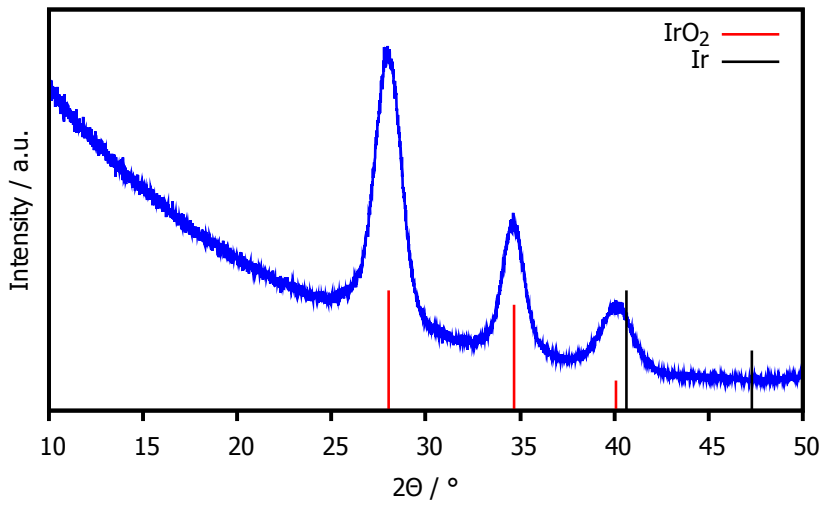

Figure S5: Grazing incidence XRD pattern of an ∼10 nm ALD IrO_2 film on oxide-terminated Si (100).

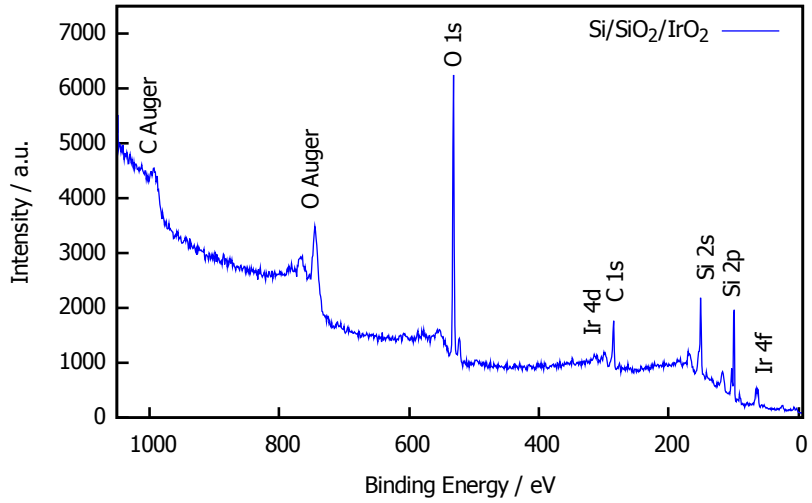

Figure S6: Survey XP spectrum, recorded from an ∼1 nm ALD IrO_2 layer on oxide-terminated Si.

Figure S6 shows a survey X-ray photoelectron spectrum of a $\leq$ 1 nm thick ALD IrO_2 layer on oxide-terminated silicon. The strong signals are the O 1s, C 1s, Si 2s, Si 2p and Ir 4f lines. The presence of adventitious carbon is a result of the sample transfer in air from the ALD to the XPS chamber. The strong Si signals signify that either the IrO_2 film is thin

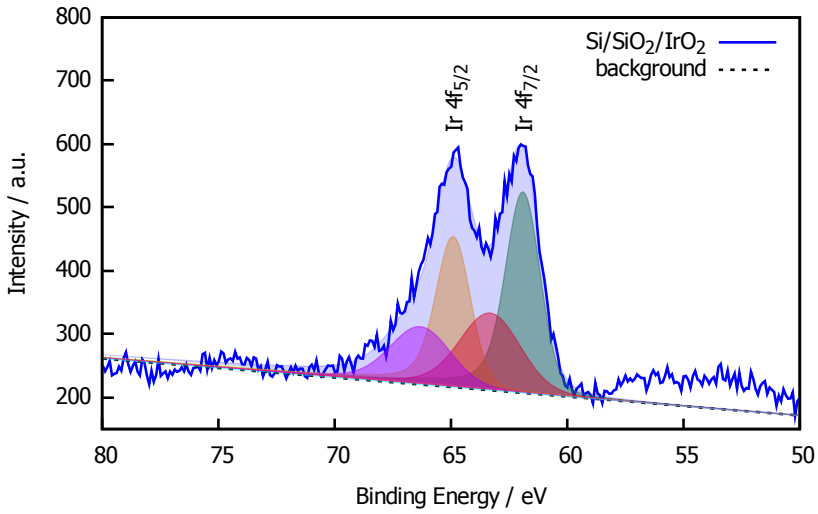

Figure S7: Detail XP spectrum of the Ir 4f signal region, recorded from an approximately 1 nm thick ALD IrO_2 layer on oxide-terminated Si. Fitting parameters according to ref[S1].

enough for photoelectrons from the underlying Si and SiO_2 to pass through it or that it is discontinuous. A detail XP spectrum of the Ir 4f region is shown in Figure S7. The Ir $4f_{7/2}$ and Ir $4f_{5/2}$ signals are centered on binding energies of 61.9 and 64.9 eV, respectively, which is in good agreement with reported values for anhydrous IrO_2.[S1] No peak or shoulder is visible at 60.8 eV, which is the reported Ir $4f_{7/2}$ binding energy of metallic Ir. The Ir 4f signal was fitted using four components as reported for IrO_2 and good fits were obtained without an added metallic component.[S1] From these results we conclude that the ALD process yields films in which the iridium is exclusively present as iridium(IV) oxide.

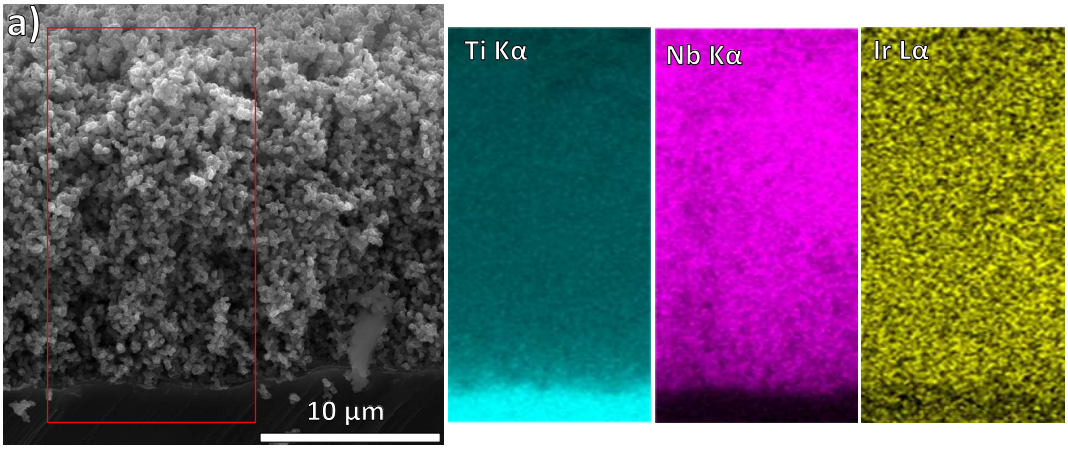

Figure S8: Cross-sectional SEM image of a Ti/C/NTO/IrO_2 electrode with EDX element distribution maps of Ti, Nb and Ir.

Electrochemical Characterization

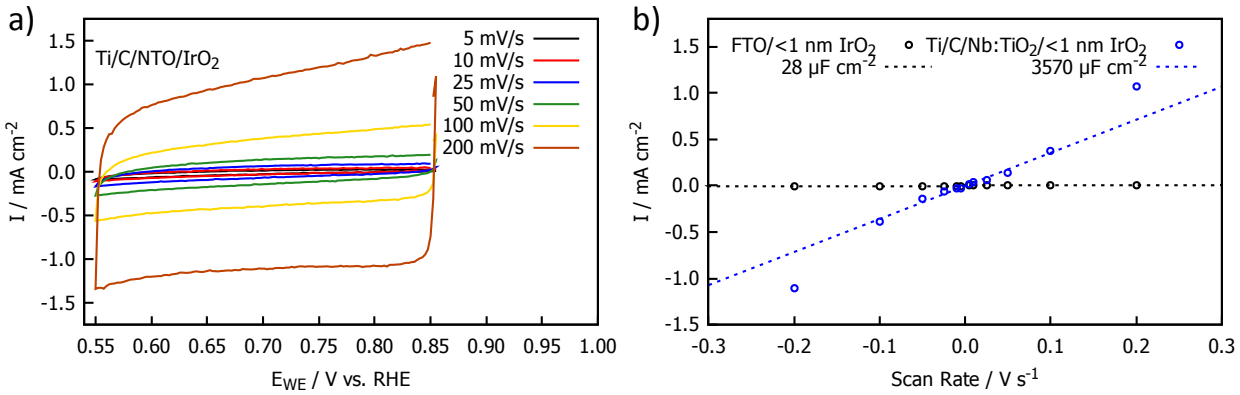

Figure S9: Cyclic voltammograms of a Ti/C/NTO/IrO_2 electrode at various scan speeds (a). Capacitive currents extracted from the CV scans in (a), compared to an FTO/IrO_2 electrode (b).

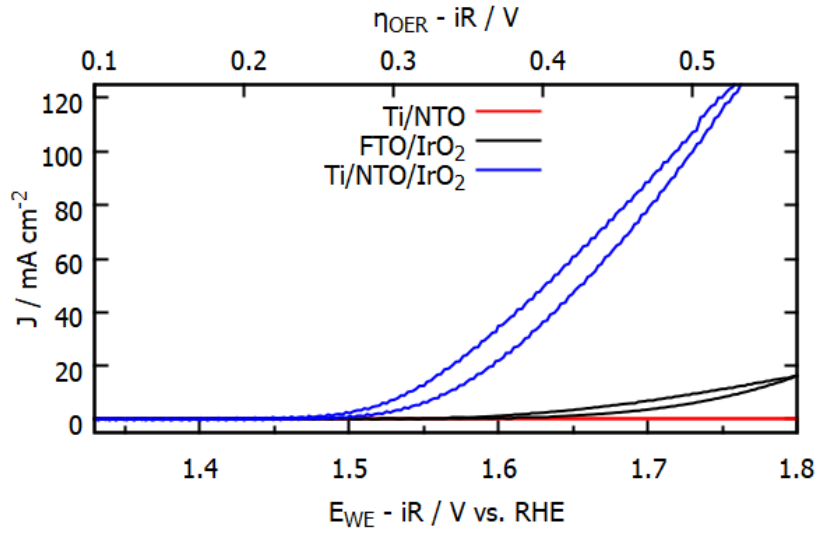

Figure S10: Uncorrected cyclovoltammograms (2nd cycle each) of Ti/C/NTO/IrO_2, Ti/C/NTO and FTO/IrO_2 electrodes recorded in 0.5 M H_2SO_4 at 20 mV s^{-1}.

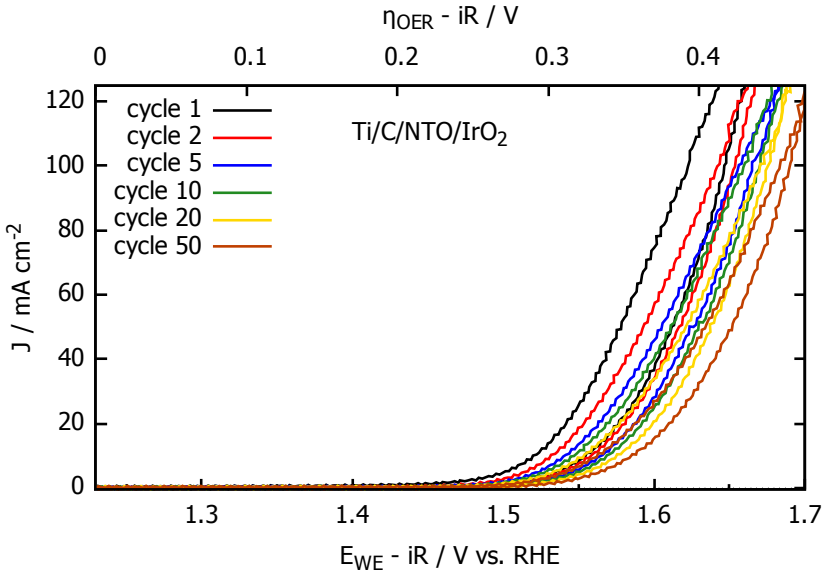

Figure S11: Cyclic voltammograms of a Ti/C/NTO/IrO_2 electrode at 20 mV s^{-1}.

Post-mortem Analysis

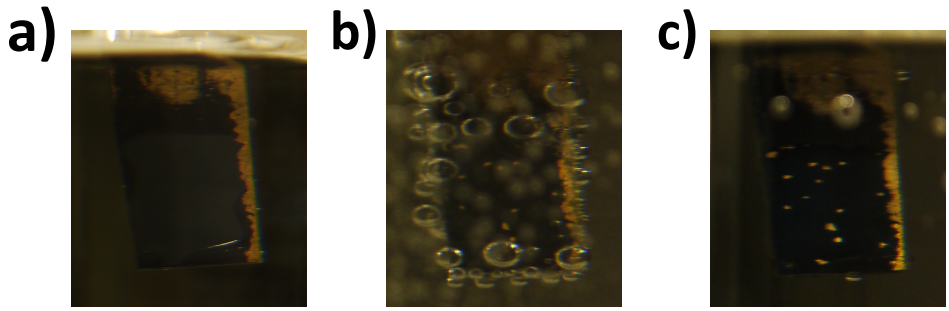

Figure S12: Photographs of a Ti/C/NTO/IrO_2 electrode in the electrolyte before (a), during (b) and after (c) water oxidation for 12 h at 100 mA cm^{-2}.

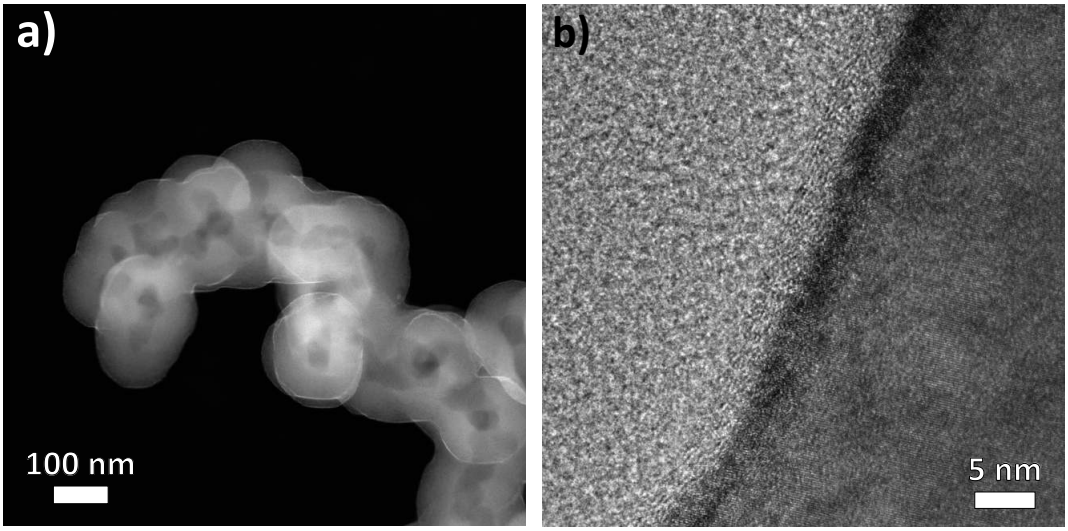

Figure S13: HAADF-STEM image of the Ti/C/NTO/IrO_2 electrode structure after the 12 h stability test (a). BF-TEM detail image of the structure from (a).

References

(S1) Freakley, S. J.; Ruiz-Esquius, J.; Morgan, D. J. The X-Ray Photoelectron Spectra of Ir, IrO2 and IrCl3 Revisited. *Surf. Interface Anal.* **2017**, *49*, 794–799.